


## Article

# Enhanced Modification between Glucose Dehydrogenase and Mediator Using Epoxy Silane Assembly for Monitoring Glucose

Tae-Won Seo <sup>1,†</sup>, Won-Yong Jeon <sup>2,3,†</sup>  and Young-Bong Choi <sup>1,\*</sup>

<sup>1</sup> Department of Chemistry, College of Science & Technology, Dankook University, Dandae-ro, Cheonan-si 31116, Chungnam, Republic of Korea; xodnjs7508@dankook.ac.kr

<sup>2</sup> School of Chemical Engineering, Translational Nanobioscience Research Center, Biomedical Institute for Convergence at SKKU (BICS), Sungkyunkwan University, Suwon 16419, Gyeonggi, Republic of Korea; powerwy@skku.edu

<sup>3</sup> Bio-Convergence Materials Research Institute, Graduate School of Management of Technology, Hoseo University, Asan 31499, Chungnam, Republic of Korea; 230275@vision.hoseo.edu

\* Correspondence: chem0404@dankook.ac.kr; Tel.: +82-41-550-3437; Fax: +82-559-7860

† These authors contributed equally to this work.

**Abstract:** Blood glucose monitoring (BGM) using disposable electrodes is commonly used in health-care diagnosis. The BGM method is not suitable for people with diabetes requiring real-time monitoring who might experience sudden hypoglycemia or hyperglycemia owing to a single measurement at a specific moment. This study aimed to achieve an enhanced stability of glucose diagnosis for continuous glucose measurement systems (CGMs). A representative mediator of a second-generation glucose sensor was synthesized and coordinated with a polymer for immobilization on an indium tin oxide (ITO) electrode. For electrode immobilization, an electrode for enhanced stability was fabricated using the silanization method. The morphological properties of the electrodes were confirmed via cyclic voltammetry (CV), impedance spectroscopy, and SEM. The loss rate of the current density was only 10.11% of the initial current after 8 d. The electrode exhibited a coefficient of determination of  $R^2 = 0.9924$ , sensitivity of  $1.5454 \mu\text{A}/\text{cm}^2 \cdot \text{mM}$ , limit of quantitation (LOQ) of  $7.604 \mu\text{M}$ , and limit of detection (LOD) of  $2.509 \mu\text{M}$  for glucose concentrations between 0.1 and 20.0 mM. The electrode system developed in this study is applicable to the CGM healthcare industry and is expected to be applicable to biofuel cells.

**Keywords:** continuous glucose monitoring; mediator; covalent binding



check for updates

**Citation:** Seo, T.-W.; Jeon, W.-Y.; Choi, Y.-B. Enhanced Modification between Glucose Dehydrogenase and Mediator Using Epoxy Silane Assembly for Monitoring Glucose. *Chemosensors* **2023**, *11*, 485. <https://doi.org/10.3390/chemosensors11090485>

Academic Editor: Yu-Ting Cheng

Received: 25 July 2023

Revised: 20 August 2023

Accepted: 27 August 2023

Published: 2 September 2023



**Copyright:** © 2023 by the authors. Licensee MDPI, Basel, Switzerland. This article is an open access article distributed under the terms and conditions of the Creative Commons Attribution (CC BY) license (<https://creativecommons.org/licenses/by/4.0/>).

## 1. Introduction

Diabetes, which is an inconvenience to human life and causes a deterioration in the quality of life, is a chronic disease that occurs when the pancreas does not produce enough insulin or when the insulin produced in the body does not work effectively. Diabetes causes a high mortality and various complications, such as heart disease, weight loss, macular degeneration, and neurological disorders. Therefore, an accurate and rapid diagnosis of diabetes is required, and research on blood glucose sensors is being actively conducted [1–3]. A blood glucose sensor, one of the biosensor types, is an analysis device that detects a change in glucose concentration. The blood glucose sensor evaluates performance metrics, such as sensitivity, response times, precision, reproducibility, responses to interference, stability, and portability. An electrochemical glucose biosensor, which is mainly used in industry, is a blood glucose measurement technique. Amperometric enzyme glucose sensors have been developed as the main technique for electrochemical glucose sensors [1,4,5]. Initially, first-generation sensors using blood oxygen as an electron transfer mediator showed inaccurate results because people have different levels of blood oxygen in their bodies. Therefore, second-generation sensors using metal complexes (artificial electron acceptors) with rapid oxidation/reduction reactions and minimal interference from other oxidation/reduction

species have been studied [1,5,6]. Because glucose oxidase (GOD), which is mainly used in amperometric glucose sensors, has good selectivity for d-glucose (substrate), it has been used in glucose sensors and diagnostic kits for a long time. However, GOD enzymes use oxygen as an electron acceptor and have a significant effect on the dissolved oxygen concentration in blood samples [7–10]. To solve this problem, glucose dehydrogenase (GDH), an enzyme that does not require an oxygen cofactor, has recently been employed. GDH can selectively oxidize glucose in the same manner as GOD. Because the electron acceptor of the GDH enzyme is not oxygen, almost no error occurred due to the oxygen content in the blood. GDH is categorized based on the type of coenzyme used. Specifically, NAD-GDH is produced with nicotinamide adenine dinucleotide (NAD), PQQ-GDH uses pyrrolo-quinoline quinone (PQQ), and FAD-GDH involves flavin adenine dinucleotide. However, due to their restricted enzymatic performance, NAD-GDH and PQQ-GDH have not been utilized in blood glucose sensors. PQQ-GDH exhibits sensitivity to icodextrin and maltose, leading to inferior glucose selectivity and diminished thermal stability, causing denaturation during prolonged storage [11]. NAD-GDH experiences an irreversible redox reaction due to NAD(P), with its enzyme selectivity diminished by the coenzyme produced through its reaction with glucosamine, xylose, fructose, maltose, and oligosaccharides [12]. FAD-GDH originates from two sources: bacteria (bFAD-GDH) and fungi (AfFAD-GDH). Specifically, bFAD-GDH, extracted from bacteria, demonstrates activity against maltose. Conversely, Af-FAD-GDH, extracted from fungi, is highly suitable for use as a glucose sensor due to its exceptional glucose selectivity, impressive thermal stability, and pH stability, although it exhibits low xylose activity [13]. In this study, we developed CGM technology using a second-generation blood glucose sensor system based on AfFAD-GDH. FAD-GDH and glucose react to produce gluconolactone and electrons [14]. Given that electrons cannot be directly transmitted to the electrode, an electron transfer medium is required.

In general, the electron transfer mediators used in second-generation sensors include ferrocene derivative, potassium hexacyanoferrate, and hexaammineruthenium trichloride, which have the advantages of a low redox potential and high electrochemical stability. However, since ferrocene has poor solubility, it is transformed into various ferrocene derivatives, such as carboxylated ferrocene or aminated ferrocene. It has been reported that these ferrocene and ferrocene derivatives have strong acute toxicity [15]. Also, potassium hexacyanoferrate (ferricyanide) and hexaammineruthenium (III) show poor electron transfer reactions with GDH [16,17]. In particular, hexaammineruthenium trichloride has a +3 charge and cannot access the active site of flavin adenine dinucleotide (FAD)-GDH, which contains a cation; therefore, it cannot serve as an electron transfer mediator. Consequently, an FAD-GDH blood glucose sensor employing an organic electron transfer mediator, such as methoxyphenazine methosulfate, has been reported [16]. Potassium hexacyanoferrate can be used as an electron transfer medium for AfFAD-GDH. However, it exhibits substantial drawbacks, such as a poor immobilization performance on the electrode. For instance, electrode elution issues arise during electrochemical sensor measurement, leading to a continuous reduction in the catalyst current. Furthermore, it exhibits sensitivity to moisture and light and is self-reducing. These factors enhance the catalytic current signal, resulting in measurement inaccuracies [18].

Therefore, Os-complex electron transfer mediators must be developed to facilitate efficient electron transfer to the electrodes through their reaction with GDH [19–23]. Most second-generation electrochemical blood glucose monitoring (BGM) devices available on the market are disposable electrodes that use metal complexes. However, the BGM is not suitable for continuous monitoring because of its poor reproducibility as a one-time electrode. In addition, drawing blood from the fingertip for repeated measurements causes pain. Moreover, because BGM cannot be continuously measured for 24 h, sudden hypoglycemia or hyperglycemia that may occur during sleep and eating cannot be identified. A continuous blood glucose sensor that continuously measures blood glucose not only avoids the pain of repetitive bloodletting but also enables “Time in Range” (TIR)

analysis [24]. In recent clinical studies, the association with the onset of complications following TIR in diabetic patients has been continuously reported. In addition, clinical trials for diabetes treatment using a continuous blood glucose system have been steadily reported, and, currently, the American Diabetes Association (ADA) recommends treatment using a continuous blood sugar system as a standard for diabetes treatment. The development of such a continuous blood glucose measurement system is necessary because it can provide an effective treatment method for diabetic patients [25]. CGM was performed to remove the blank BGM measurement period. Accordingly, CGM sensors modified with materials such as enzymes and electron transfer mediators on the working electrode surfaces of carbon, silver, gold, platinum, and indium tin oxide (ITO) have been developed [26–32]. Representative electrochemical CGM technologies currently being developed are divided into the non-invasive CGM (NI-CGM) and the minimally invasive CGM (MI-CGM). However, NI-CGM is not developed practically because it shows a low mean absolute relative difference (MARD) value. MI-CGM technology with excellent MARD is generally available from 7 to 14 days, so it has been developed. Therefore, in this study, an osmium complex with an excellent LOD, LOQ, and MARD was used as an electron transfer medium, and CGM technology that can be used for a long time was developed by effectively immobilizing the electron transfer medium and enzyme on the electrode [33,34]. Representative methods for immobilizing electron transfer mediators and enzymes on electrode surfaces include adsorption, covalent bonding, crosslinking, entrapment in a porous matrix, and polymer film coating [35–38]. CGM electrodes with immobilized enzymes and electron transfer mediators can be recovered and reused in the liquid state because of their high stability in organic solvents, wide range of temperatures, and exposure to microorganisms [38–40]. Additionally, given that the electron transfer mediators are not eluted from the electrode surface, a constant catalytic current can be maintained without a signal reduction [38–43]. In this study,  $[\text{Os}(\text{dmo-bpy})_2\text{Cl}_2]^{0/+}$  was synthesized through the coordination of ammonium hexachloroosmate (IV) with 4,4-dimethoxy-2,2-bipyridine(dmo-bpy). The copolymerized polyacrylamide–polyvinylimidazole (PAA–PVI) was then coordinated with PAA–PVI– $[\text{Os}(\text{dmo-bpy})_2\text{Cl}]^{+/2+}$  as the final mediator [44–47]. The synthesized osmium electron transfer mediator has a lower oxidation–reduction potential (–0.01 V) than previously reported osmium complexes [48]. A sensor operating at a low voltage of less than 0.1 volt can easily avoid signal interference from electrochemical interfering species present in living organisms without a separate selective membrane [49]. Subsequently, an ITO electrode bonded with 3-glycidoxypropyltrimethoxysilane (GOPTS) via hydrolysis and condensation was conjugated with PAA–PVI– $[\text{Os}(\text{dmo-bpy})_2\text{Cl}]^{+/2+}$ . Finally, a GDH/Mediator–Silane–ITO electrode was fabricated by immobilizing GDH on the surface of the PAA–PVI– $[\text{Os}(\text{dmo-bpy})_2\text{Cl}]$ –Silane–ITO electrode [50–55].

## 2. Materials and Methods

### 2.1. Chemicals and Reagents

GDH (FAD-dependent GDH-584 U/mg) was purchased from Toyobo Co., Ltd. (Osaka, Japan). Ammonium hexachloroosmate (IV), dmo-bpy, 1-vinylimidazole, acrylamide, ammonium persulfate, N,N,N',N'-tetramethylethylenediamine, poly(ethylene glycol) diglycidyl ether (PEGDEG), D-(+)-glucose, GOPTS, and toluene were purchased from Sigma–Aldrich Co. (Milwaukee, WI, USA). The analytical reagents were used without further purification. Phosphate-buffered saline (1XPBS pH7.4), sodium dihydrogen phosphate ( $\text{NaH}_2\text{PO}_4$ , 4.3 mM), sodium hydrogen phosphate ( $\text{Na}_2\text{HPO}_4$ , 15.1 mM), sodium chloride (NaCl, 140 mM), and all other solutions were prepared using deionized (DI) Milli-Q water (Millipore, Tokyo, Japan).

### 2.2. GDH/Mediator–Silane–ITO Electrode Fabrication

#### 2.2.1. PAA–PVI Synthesis

The PAA–PVI (7:1) polymer was synthesized as described previously [45]. Acrylamide (4.967 g, 0.07 mol) and 1-vinylimidazole (0.905 mL, 0.1 mol) were stirred in a 250 mL beaker

with DI water (150 mL) as a solvent. This solution was heated to 40 °C, and a mixed solution of ammonium persulfate (0.2 g) and N,N,N',N'-tetramethylethylenediamine (0.21 mL) dissolved in 30 mL of DI water was slowly added dropwise. After a sufficient reaction time, the solution was added dropwise to 500 mL of acetone to precipitate the polymer. After vacuum filtration, vacuum drying was performed for 1 d.

#### 2.2.2. Os(dmo-bpy)<sub>2</sub>Cl<sub>2</sub> Synthesis

Os(dmo-bpy)<sub>2</sub>Cl<sub>2</sub> was synthesized as previously described [56]. Ammonium hexachloroosmate (1 g, 2.28 mmol) and dmo-bpy (1.08 g, 5.02 mmol) were stirred and refluxed for 1 h (180 °C) with 100 mL of ethylene glycol in a round-bottom flask. After the reaction was complete, sodium hydrosulfite (15.9 g, 91.2 mmol) dissolved in DI water (350 mL) was added to the product, and this mixture was stored in a refrigerator at 4 °C for 24 h. Subsequently, the reduced product was obtained via vacuum filtration using a 0.45 µm nylon filter. The final product was used after completely drying in an oven at 40 °C for 2 d.

#### 2.2.3. PAA-PVI-[Os(dmo-bpy)<sub>2</sub>Cl] Synthesis

PAA-PVI-[Os(dmo-bpy)<sub>2</sub>Cl] was synthesized as described previously [56]. The PVI polymer powder (0.0323 g, 5 eq) and Os(dmo-bpy)<sub>2</sub>Cl<sub>2</sub> (0.0658 g, 1 eq) were stirred and refluxed for 24 h (120 °C) with 20 mL of ethylene glycol in a nitrogen-saturated round-bottom flask. Then, a mixture of 50 mL of acetone and 200 mL of diethyl ether was added dropwise to obtain a precipitate. The precipitate was dissolved in 50 mL of DI water. The solution was concentrated using ultrafiltration disks (10 kDa). Finally, the concentrated solution was re-precipitated by adding it dropwise into 5.0 L of diethyl ether, and then the powder was stored in a vacuum oven for complete drying.

#### 2.2.4. GDH/Mediator-Silane-ITO Electrode Preparation

Silanization was performed as previously described to prepare the enzyme electrodes [50,51]. Scheme 1 shows the silanized chemical structure and the hydrolysis and condensation reactions on the ITO electrode. First, a 4% (v/v) solution was prepared by mixing 12 mL of GOPTS with 30 mL of toluene. ITO electrodes were cleaned with a piranha solution (H<sub>2</sub>SO<sub>4</sub>:H<sub>2</sub>O<sub>2</sub>:DW = 4:1:1) and surface hydroxy-modified, then they were placed in the GOPTS solution and allowed to react at 25 °C for 1 d.

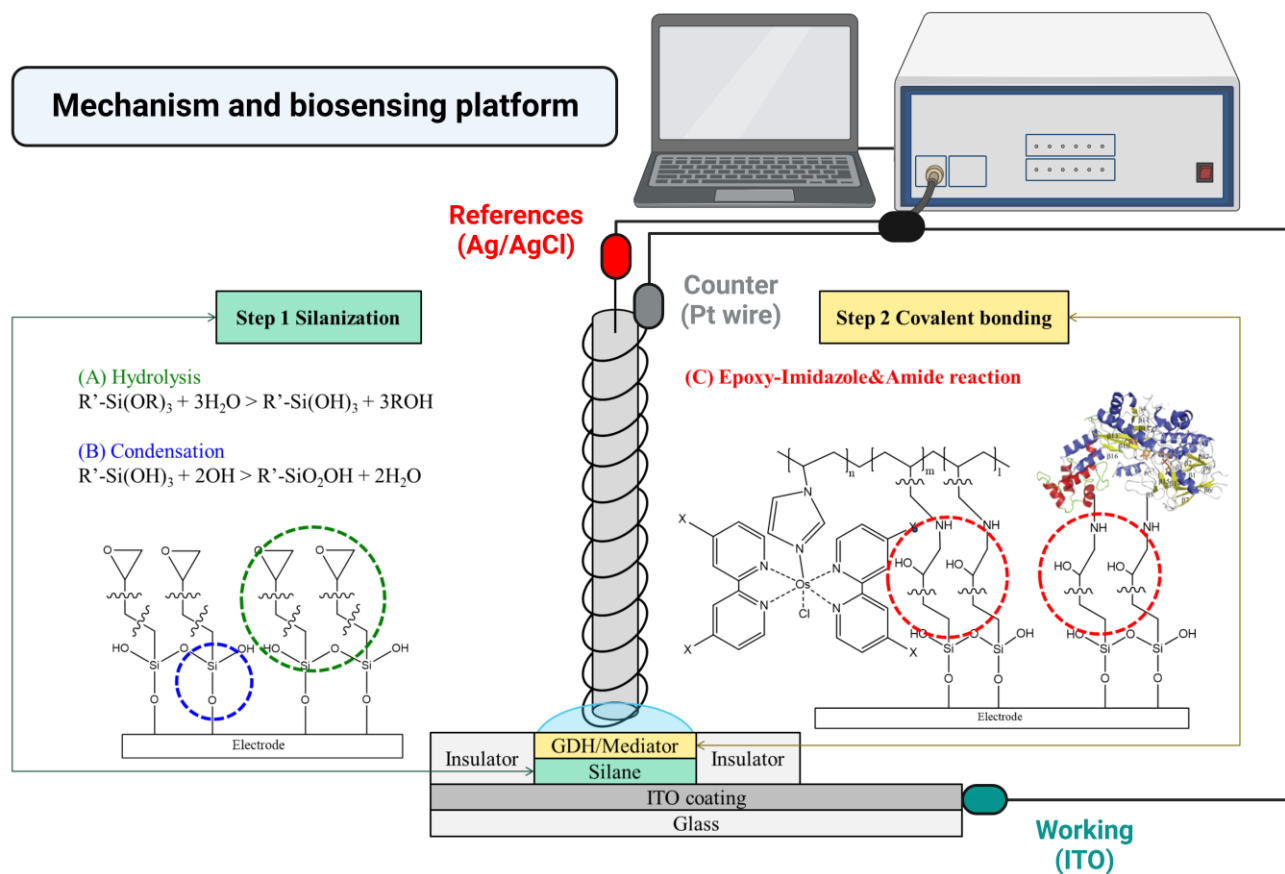
Second, the mixed solution (10 µL; 4:4:1, v/v/v) of GDH (40 mg/mL), a mediator (10 mg/mL), PAA-PVI-[Os(dmo-bpy)<sub>2</sub>Cl], and a crosslinker (10 mg/mL) named PEGDGE was cast and completely dried (at 25 °C for 1 d) onto the silanized ITO electrode. In this process, the amine of the enzyme and mediator can be coordinated with the epoxy of GOPTS on the ITO electrode [52–55].

Finally, the GDH/Mediator-Silane-ITO electrodes were cleaned via ultrasonication for 1 min to remove the physical absorption substrates. Subsequently, the electrodes were completely dried using nitrogen gas. All experiments were conducted after stabilization in a refrigerator for 1 d.

### 2.3. Electrochemical Analysis of GDH/Mediator-Silane-ITO Electrodes

A CHI 660 B potentiostat (CH Instruments Inc., Austin, TX, USA) was used for all electrochemical measurements. A platinum wire (platinum wire, 0.5 mm diameter, 99.99% metal basis) (Aldrich Chem. Co., Milwaukee, WI, USA) rolled in a Ag/AgCl electrode (ESA, EE009) was used as the counter and reference electrodes. ITO (7 cm × 2.5 cm) was used as the working electrode (contact area: 0.2826 cm<sup>2</sup>). Cyclic voltammetry (CV) was used to evaluate the electrochemical properties of glucose and GDH/Mediator-Silane-ITO electrodes [56–59]. Electrochemical impedance spectroscopy (EIS) was used to characterize bare ITO, Silane-ITO, Mediator-Silane-ITO, and GDH/Mediator-Silane-ITO electrodes. For EIS measuring, a 40 µL mixed solution (1:1, v/v) of 2 mM potassium hexacyanoferrate (II) trihydrate and 2 mM potassium hexacyanoferrate (III) was used. The frequency range was 10<sup>4</sup>–10<sup>−1</sup> Hz, and the AC amplitude was 5 mV. Amperometric I-t curves were used to

measure glucose levels and long-term stability. Additionally, interference species, such as ascorbic acid (AA), dopamine (DA), and uric acid (UA), which can exist in the body, are typically tested using the I–t curve technique.



**Scheme 1.** Fabrication and mechanism of electrode and biosensing process.

### 3. Results and Discussion

#### 3.1. Electrodes' Characterization

##### 3.1.1. Morphological Properties

Figure 1 shows the results of FE-SEM (Field-Emission Scanning Electron Microscope) measurements after platinum coating to confirm the morphological properties of the electrodes. Figure 1a,b show bare ITO- and GOPTS-coated electrodes, respectively. Figure 1a assumes that no substances were observed on the surface of ITO after piranha solution cleaning. A comparison of the results shown in Figure 1a,b confirms that the surface modification of the GOPTS was successful and uniform. The uniform adsorbate in Figure 1b is presumed to be aggregated through the hydrolysis and condensation reaction of the hydroxyl functional group of the ITO electrode and the epoxy silane compound, as in step 1 of Scheme 1. Figure 1c presents the results after the immobilization of PAA–PVI–[Os(dmo–bpy)<sub>2</sub>Cl]. Consequently, the PAA–PVI–[Os(dmo–bpy)<sub>2</sub>Cl] mediator was attached and covered on the silanized ITO electrode. The data derived under enzyme-included conditions, as shown in Figure 1d, signify the aggregation of macromolecules on the Silane–ITO electrode. Most of the mediators are aggregated with the enzymes, and a few mediators are assumed to spread over the surface. The results revealed the shape of the macromolecules on the surface and confirmed that immobilization was successful.



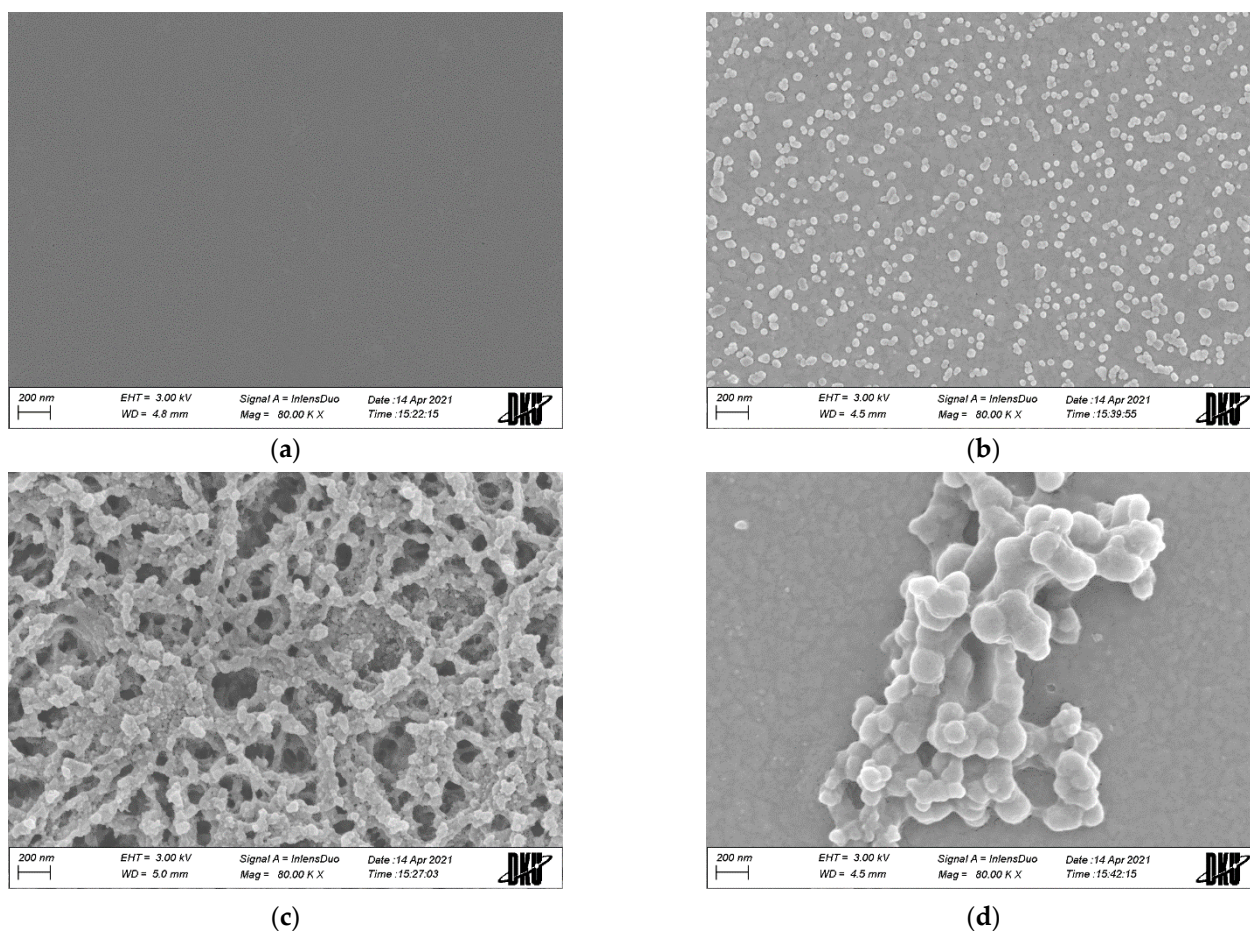


**Figure 1.** FE-SEM of (a) bare ITO (80 K); (b) Silane-ITO (80 K); (c) Mediator-Silane-ITO (80 K); and (d) GDH/Mediator-Silane-ITO (80 K) electrodes.

### 3.1.2. Spectroscopic Properties

A UV-Vis spectrophotometer was employed to verify the synthesis of the mediator, as illustrated in Figure 2. UV-Vis spectroscopic results for all compounds were obtained in DI water. Figure 2a displays the outcome of the polymerization of PAA-PVI from 1-vinylimidazole and acrylamide. In imidazole, a  $\pi$ - $\pi^*$  electron transition was observed at a relatively long wavelength of 230 nm due to delocalized electrons [60]. Acrylamide displayed an absorption wavelength of 205 nm for  $\pi$ - $\pi^*$  electron transition attributable to the carbonyl and c=c double bonds [61]. The synthesized PAA-PVI compound absorbed light at a short wavelength of 215 nm, and it was determined that the absorption wavelengths of 230 nm of imidazole and 205 nm of acrylamide merged and appeared as a single peak at 215 nm, corresponding to the intermediate value [62]. Figure 2b depicts the resulting coordinates of Os(dmo-bpy)<sub>2</sub>Cl<sub>2</sub> and PAA-PVI. Os(dmo-bpy)<sub>2</sub>Cl<sub>2</sub> is an organometallic complex encompassing a transition metal, and the d-d transition, metal to ligand charge transfer (MLCT), and ligand to metal charge transfer (LMCT) can be observed depending on the type of ligand linked to the central metal. The synthesized PAA-PVI-Os(dmo-bpy)<sub>2</sub>Cl demonstrated an MLCT transition that was spin-allowed at 370 nm, as observed for Os(dmo-bpy)<sub>2</sub>Cl<sub>2</sub>, and confirmed that the MLCT was spin-allowed at 210 nm. Moreover,  $\pi$ - $\pi^*$  electron transitions of the ligand (LLCT) were confirmed at 225, 275 nm (Os(dmo-bpy)<sub>2</sub>Cl), and 215 nm (PAA-PVI) [63]. Hence, PAA-PVI-Os(dmo-bpy)<sub>2</sub>Cl was observed at the same wavelength as the respective absorption wavelengths of PAA-PVI and Os(dmo-bpy)<sub>2</sub>Cl<sub>2</sub>, confirming the successful synthesis of the final compound.

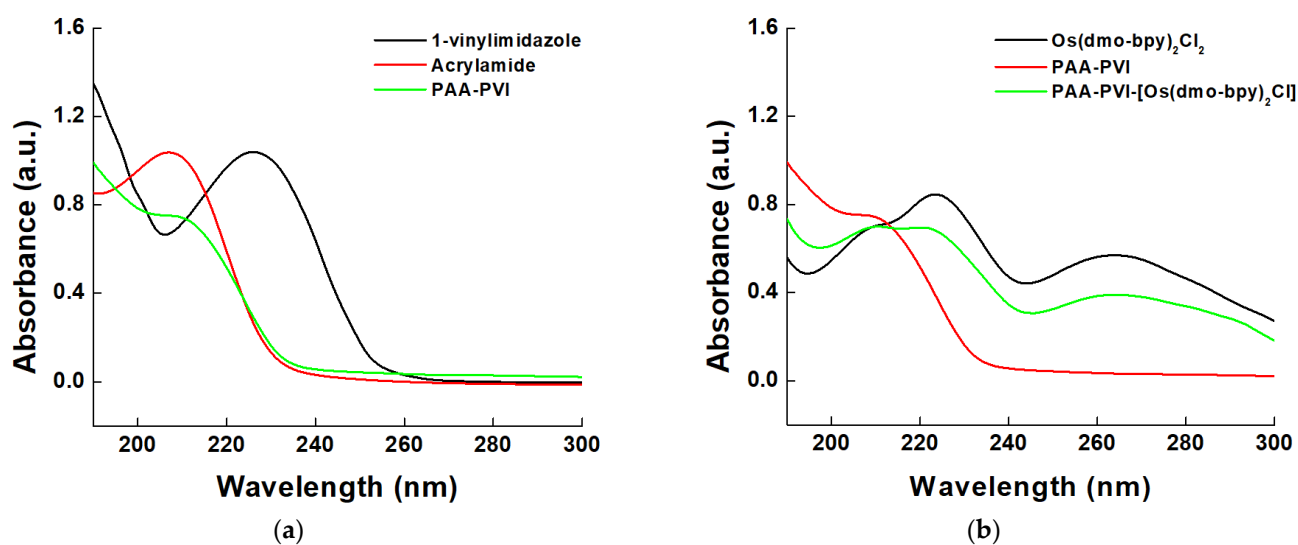


Figure 2. UV-vis spectra result of (a) polymerization and (b) final mediator (PAA-PVI-[Os(dmo-bpy)<sub>2</sub>Cl]).

### 3.1.3. Electrochemical Properties

Figure 3a shows a cyclic voltammogram of the current density according to the change in the scan rate (0.01–1 V/s) to check the performance of the GDH/Mediator–Silane–ITO electrode as an electron transfer mediator and the diffusion effect of the solution phase [57–59]. The potential of the maximum redox current did not change significantly with increasing scan rate; only the current density showed a constant tendency to increase. This implied that PAA-PVI-[Os(dmo-bpy)<sub>2</sub>Cl] was “stably” immobilized on the ITO electrode. This also indicates that the quasi-reversible redox peak of the medium was reversible ( $E = -0.0315$  V) and suitable for use in electrochemical analysis. Figure 3b shows the change in the current density as the scan rate increases. The maximum oxidation-reduction current showed excellent linearity ( $I_{pa}$   $R^2 = 0.99833$  and  $I_{pc}$   $R^2 = 0.99882$ ), indicating that no reaction occurred owing to the diffusion of the immobilized electron transfer mediator during the electron transfer process [64].

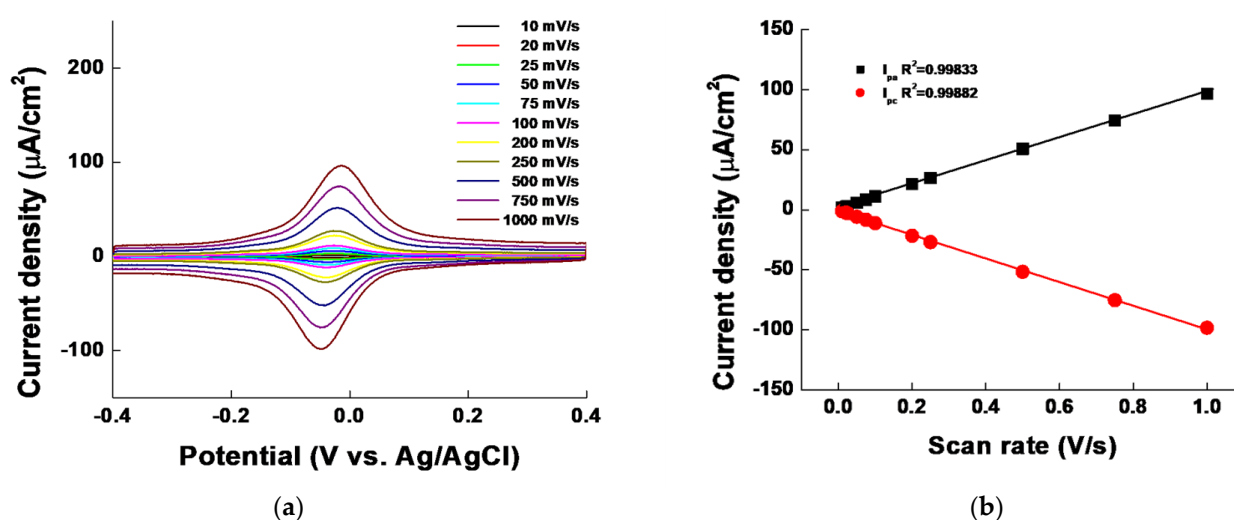
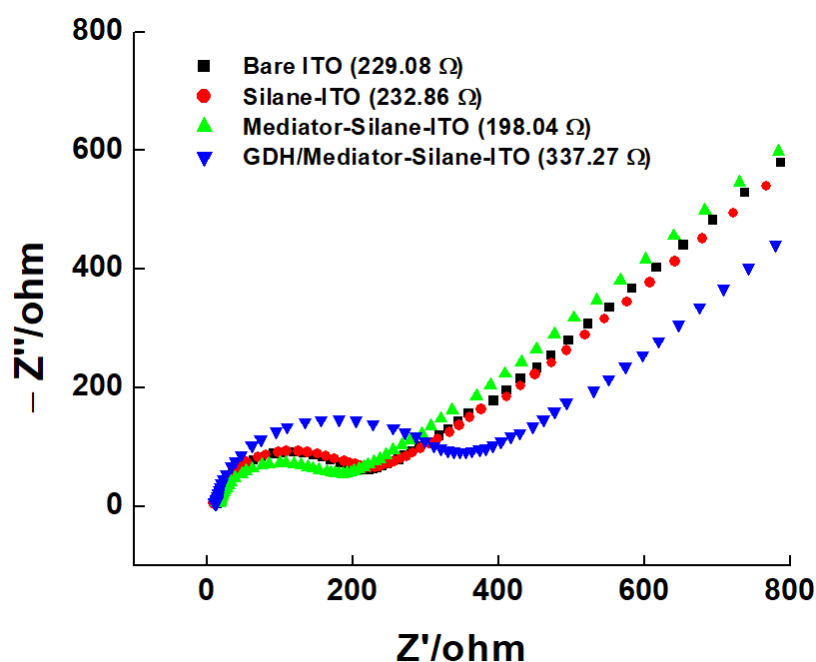


Figure 3. (a) Cyclic voltammogram and (b) redox scan rate curve of the GDH/MET–Silane–ITO electrode within a scan rate range of 0.01–1.0 V/s.

Figure 4 shows the EIS results of the electrodes. The bare ITO, Silane–ITO, Mediator–Silane–ITO, and GDH/Mediator–Silane–ITO electrodes were measured using 2 MM of

$K_3[Fe(CN)_6]/K_4[Fe(CN)_6]$  in 0.5 M of KCl, and the resistance ( $R_s$ ) of the solution was  $13.0 \Omega$ . The bare ITO electrode showed a surface resistance of  $229.08 \Omega$ , and the electrode treated with surface silane showed a slight increase of  $232.86 \Omega$  in the resistance owing to the absorbance of the SAM process. When the mediator was combined with a silane-treated ITO electrode, the decrease in surface resistance due to the transition metal resulted in an EIS surface resistance of  $198.04 \Omega$ . Finally, a GDH immobilized condition (GDH/Mediator–Silane–ITO electrode) showed the resistance increasing to  $337.27 \Omega$  owing to the large molecular size of the enzyme [65]. These results show a trend similar to that of the previously identified SEM images in Figure 1, indicating that our electrodes are successfully fabricated.



**Figure 4.** Nyquist plot for bare ITO (black squares), Silane–ITO (red circles), Mediator–Silane–ITO (green triangles), and GDH/Mediator–Silane–ITO (blue inverted triangles).

### 3.2. Electrodes' Performances

#### 3.2.1. Glucose Measurements

The developed GDH/Mediator–Silane–ITO electrodes were used for testing glucose levels of 0.1, 0.5, 1.0, 2.5, 5.0, 10.0, and 20.0 mM (1XPBS pH 7.4) using CV and I-t curves. The CV curves in Figure 5a show stable catalytic currents at various glucose concentrations on the GDH/Mediator–Silane–ITO electrodes. An increase in glucose concentration led to a bias of the redox mediator peak toward the oxidation catalytic current. In addition, the I-t curves in Figure 5b show an increasing current (potential of 0.1 V) with increasing glucose levels. Based on the inset of Figure 5b, a coefficient of determination ( $R^2$ ) of 0.9911, sensitivity of  $1.5454 \mu A/cm^2 \cdot mM$ , LOD of  $2.509 \mu M$ , and LOQ of  $7.604 \mu M$  were obtained. The log dependence of glucose shows a logarithmic relationship as the concentration increases according to the diffusion law, and the enzyme catalysis, electrochemical reaction, and nucleic acid amplification show log dependence. In this study, log-dependent data were shown because glucose was measured by the effect of enzyme catalysis and electrochemical reaction. Correcting this with a linear regression model through an algebraic method has the advantages of not affecting the result value, simplifying the result, and making it easy to recognize [66,67].



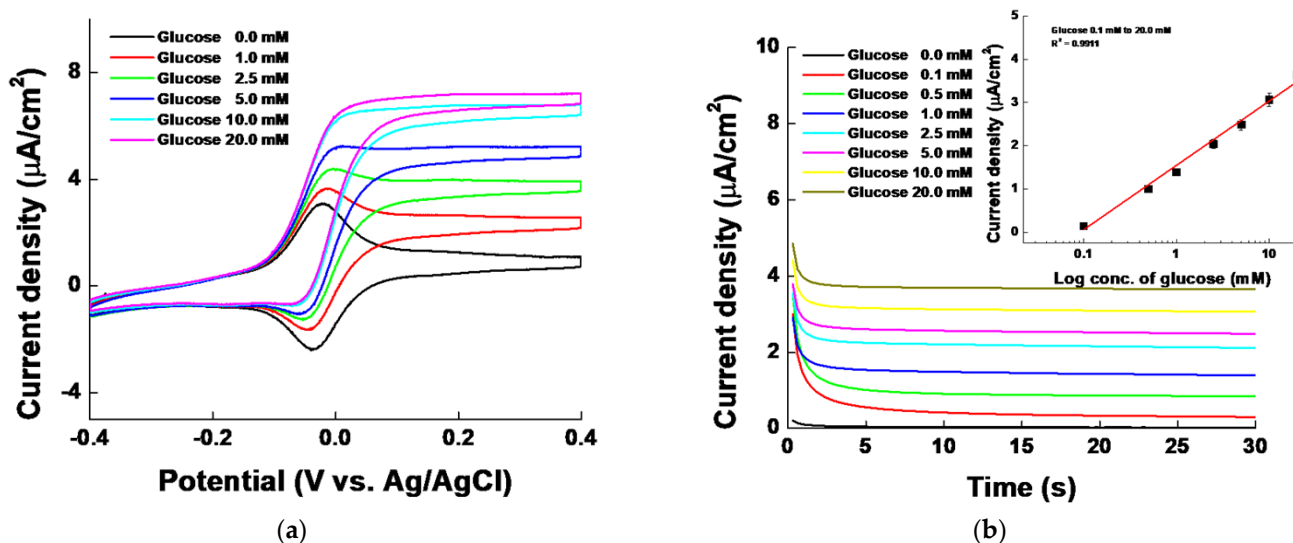


**Figure 5.** (a) Cyclic voltammogram and (b) I–t curves of the GDH/Mediator–Silane–ITO electrode with a glucose concentration range of 0.0–20.0 mM. Inset shows the calibration curve of the I–t curve after 30 s.

Generally, the LOD and LOQ must be verified by repeatedly measuring the background signal to obtain the signal-to-noise ratio [68]. In this study, the LOD and LOQ were calculated using a standard deviation ( $0.001175 \mu\text{A}/\text{cm}^2$ ) and a low-concentration origin correction calibration curve ( $Y = aX$ ,  $Y = 1.5454X$ ) of 0.1–1.0 mM through five background signal measurements, as presented in Table 1, according to the International Council for Harmonisation of technical requirements for pharmaceuticals for human use/validation of analytical procedures Code: Q2(R2) (ICH Q2(R2)) guideline. As a result, the LOD = 0.007604 mM and the LOQ = 0.002509 mM, confirming the possibility of low-concentration glucose verification. To confirm the time–current response to the glucose concentration, I–t curves were obtained by spiking 1 mL of a 100 mM glucose solution (1XPBS pH7.4) at an interval of 50 s (Figure S1). The glucose concentration in the final solution was maintained until it reached 16.67 mM. The GDH/Mediator–Silane–ITO electrode showed that the signal value increased each time the 100 mM glucose solution was spiked, and the signal was maintained without dropping, even when the measurement was performed for 50 s. However, the GDH/Mediator–ITO electrode without silanization showed an unstable glucose response and stability. This suggests that the developed GDH/Mediator–Silane–ITO electrode could be used for continuous glucose monitoring (CGM) measurements.

**Table 1.** LOD and LOQ values using the standard deviation of the background signal according to the ICH Q2(R2) guidelines.

Test Number	BKG Signal	Net. Signal	ICH Q2(R2) Guideline	0.1–1 mM net. Calibration Curve
1	$-7.31 \times 10^{-9}$	$2.52 \times 10^{-2}$	LOD = 3.3 s/m	$Y = 1.5454X$
2	$-6.98 \times 10^{-9}$	$2.47 \times 10^{-2}$	LOQ = 10 s/m	$R^2 = 0.9777$
3	$-7.02 \times 10^{-9}$	$2.48 \times 10^{-2}$	Standard deviation (s) = $0.001175 \mu\text{A}/\text{cm}^2$ Sensitivity (m) = $1.5454 \mu\text{A}/\text{cm}^2 \cdot \text{mM}$	LOQ = 0.007604 mM
4	$-6.96 \times 10^{-9}$	$2.46 \times 10^{-2}$		LOD = 0.002509 mM
5	$-7.84 \times 10^{-9}$	$2.77 \times 10^{-2}$		

### 3.2.2. Sensor Testing

Figure 6a shows the I–t curves at a potential 0.1 V of 0.05 mM AA, 0.1 mM UA, 0.1 mM DA, 0.1 mM glucose, and 1.0 mM glucose, which are physiological electrochemical reaction species, to evaluate the interference effect on the GDH/Mediator–Silane–ITO electrode [69–72]. The findings indicated that the GDH/Mediator–Silane–ITO electrode

responded exclusively to glucose concentrations of 0.1 and 1.0 mM. The bar graph in Figure 6b shows the current density of the I-t curves shown in Figure 6a at 30 s. Interfering substances with high oxidation potentials did not affect the oxidation current values at the oxidation potential of the GDH/Mediator–Silane–ITO electrode.

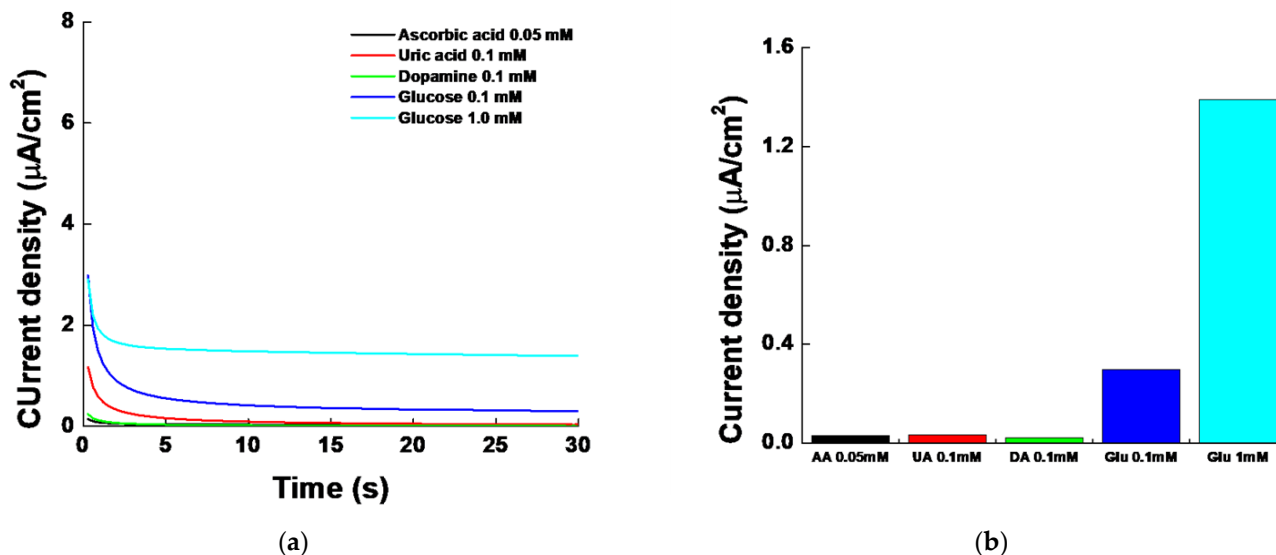


**Figure 6.** (a) I-t curve and (b) bar graph for testing the interference effect of 0.05 mM of ascorbic acid (black), 0.1 mM of uric acid (red), 0.1 mM of dopamine (green), 0.1 mM of glucose (blue), and 1.0 mM of glucose (sky blue). The bar graph indicates the current density of the I-t curves at 30 s.

For use in CGM, the long-term response stability was investigated for 8 d (Figure 7). The current density was evaluated using identical electrodes in 5 mM of glucose (1XPBS pH7.4). After the current measurements were recorded, the electrodes were rinsed in distilled water and stored in a desiccator ( $N = 5$ ). As a result, the relative change/% of the current density for 8 d was 10.11%, implying that the current density of the GDH/Mediator–Silane–ITO electrode decreased insignificantly. However, the stability of the GDH/Mediator–ITO electrode without silanization (red circles) decreased dramatically. This indicates that our silanization process significantly contributed to the firm immobilization of the GDH/Mediator on the ITO electrodes, thus aiding in the maintenance of long-term stability. Previous studies with objectives analogous to ours are consolidated in Table 2 [73]. Compared to the electrodes reported in other studies, our GDH/Mediator–Silane–ITO electrode displayed superior stability. This study confirmed that the developed electrode had excellent stability in terms of the signal response, LOD, and stability and confirmed its applicability to the CGM system of next-generation glucose sensors.

**Table 2.** Comparison of stability performance of glucose sensing electrodes.

Reports	Electrode Type	Dynamic Range	LOD	Sensitivity	Continuous Glucose Monitoring
[74]	GOX/PEDOT/Carbon	36–432 mg/dL	N/A	N/A	24% lost for 7 d
[75]	GOX/TIF/Carbon	90–450 mg/dL	N/A	N/A	25% lost for 60 h
[76]	GOX/MPA/Au	50–400 mg/dL	N/A	N/A	20% lost for 7 d
[77]	GOX/PPD	18–252 mg/dL	21 $\mu\text{M}$	0.353 $\mu\text{A}/\text{mM}$	3% lost for 8 h
Our study	GDH/Mediator–Silane–ITO	1.8–360.3 mg/dL (0.1–20.0 mM)	2.509 $\mu\text{M}$	1.5454 $\mu\text{A}/\text{cm}^2\cdot\text{mM}$	10.11% lost for 8 d

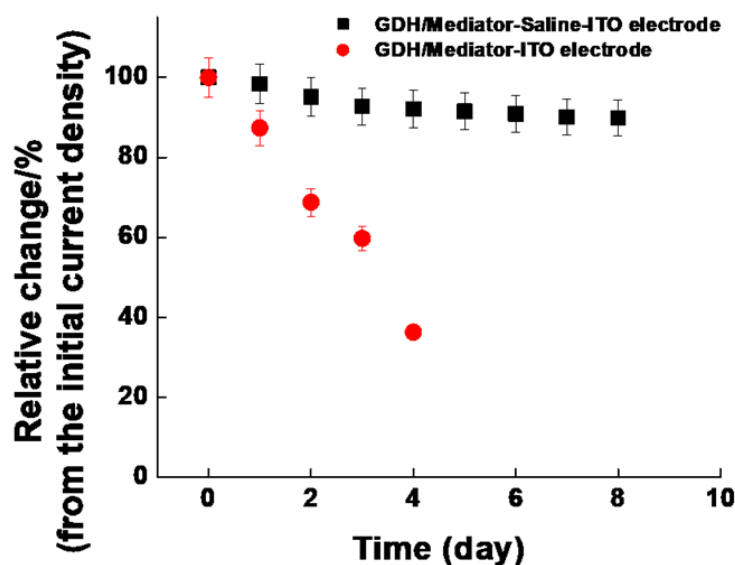


**Figure 7.** Relative change/% of GDH/Mediator–Silane–ITO (black square) and GDH/Mediator–ITO (red circle) electrodes for 8 d (GDH/Mediator–Silane–ITO electrode; %RSD = 2.73%).

#### 4. Conclusions

Among glucose biosensors based on electrochemistry, the BGM system has disadvantages, such as the use of one-time electrodes, pain during blood collection, and shock due to rapid blood glucose changes. To solve these problems, we developed GDH/Mediator–Silane–ITO electrodes in which the electron transfer mediator and GDH were stably immobilized by GOPTS in the ITO electrode. Our easy method of silanization extended the measurement time dramatically. The performance of the immobilized GDH/Mediator–Silane–ITO electrode had good linearity ( $R^2 = 0.9911$ ) at concentrations of glucose between 0.1 and 20.0 mM. The LOD (2.509  $\mu\text{M}$ ) and %RSD (2.73%) of our electrode indicated a good performance. However, the loss rate (10.11%) for 8 days was not better than the loss rate (3%) of the GOX/PPD electrode in a previous report [77]. We believe that using a hydrogel or a suitable polymer for an assembled film will increase the stability of the GDH in our electrode system. It is also expected to take the lead in extending the operation time. The future direction of the work will be trying to change size and shape of our electrode system for compatibility and applicability with animal models and clinical trials. Finally, we believe that our effort will decrease the blood draw pain of diabetic patients and allow for the real-time monitoring of glucose for avoiding sudden shock.

**Supplementary Materials:** The following supporting information can be downloaded at: <https://www.mdpi.com/article/10.3390/chemosensors11090485/s1>, Figure S1: I-t curve of GDH/Mediator–Silane–ITO (black line) and GDH/Mediator–ITO (red line) electrodes according to glucose addition (Total glucose concentrations: 50 s (1.96 mM), 100 s (3.85 mM), 150 s (5.66 mM), 200 s (7.41 mM), 250 s (9.09 mM), 300 s (10.71 mM), 350 s (12.28 mM), 400 s (13.79 mM), 450 s (15.25 mM), and 500 s (16.67 mM)).

**Author Contributions:** Conceptualization, W.-Y.J. and Y.-B.C.; methodology, W.-Y.J. and Y.-B.C.; validation, W.-Y.J., T.-W.S. and Y.-B.C.; formal analysis, T.-W.S.; investigation, T.-W.S.; data curation, W.-Y.J. and Y.-B.C.; writing—original draft preparation, W.-Y.J. and Y.-B.C.; writing—review and editing, W.-Y.J. and Y.-B.C.; visualization, T.-W.S.; supervision, Y.-B.C.; project administration, Y.-B.C.; funding acquisition, W.-Y.J. All authors have read and agreed to the published version of the manuscript.

**Funding:** This work was supported by the National Research Foundation of Korea (NRF) grants funded by the Korean government (MSIT) (Nos. 2017R1A6A3A11035249, 2020R1C1005523, and 2022R111A1A01062663). This study was supported by the SKKU Global Research Platform Research Fund (Sungkyunkwan University, 2023).

**Institutional Review Board Statement:** Not applicable.

**Informed Consent Statement:** Not applicable.

**Data Availability Statement:** Not applicable.

**Acknowledgments:** Scheme 1 was created using Biorender (Bio-Render, Toronto, Canada).

**Conflicts of Interest:** The authors declare no conflict of interest.

## References

1. Heller, A.; Feldman, B. Electrochemical Glucose Sensors and Their Applications in Diabetes Management. *Chem. Rev.* **2008**, *108*, 2482–2505. [[CrossRef](#)]
2. Reach, G.; Wilson, G.S. Can Continuous Glucose Monitoring Be Used for the Treatment of Diabetes. *Anal. Chem.* **1992**, *64*, 381A–386A. [[CrossRef](#)]
3. Turner, A.P.; Chen, B.; Piletsky, S.A. In Vitro Diagnostics in Diabetes: Meeting the Challenge. *Clin. Chem.* **1999**, *45*, 1596–1601. [[CrossRef](#)]
4. Kobos, R.K. Enzyme-Based Electrochemical Biosensors. *TrAC Trends Anal. Chem.* **1987**, *6*, 6–9. [[CrossRef](#)]
5. Chen, C.; Xie, Q.; Yang, D.; Xiao, H.; Fu, Y.; Tan, Y.; Yao, S. Recent Advances in Electrochemical Glucose Biosensors: A Review. *RSC Adv.* **2013**, *3*, 4473–4491. [[CrossRef](#)]
6. Wang, J. Glucose Biosensors: 40 Years of Advances and Challenges. *Electroanalysis* **2001**, *13*, 983–988. [[CrossRef](#)]
7. Wang, J. Electrochemical Glucose Biosensors. *Chem. Rev.* **2008**, *108*, 814–825. [[CrossRef](#)]
8. Horaguchi, Y.; Saito, S.; Kojima, K.; Tsugawa, W.; Ferri, S.; Sode, K. Engineering Glucose Oxidase to Minimize the Influence of Oxygen on Sensor Response. *Electrochim. Acta* **2014**, *126*, 158–161. [[CrossRef](#)]
9. Tang, Z.; Louie, R.F.; Lee, J.H.; Lee, D.M.; Miller, E.E.; Kost, G.J. Oxygen Effects on Glucose Meter Measurements with Glucose Dehydrogenase- and Oxidase-Based Test Strips for Point-of-Care Testing. *Crit. Care Med.* **2001**, *29*, 1062–1070. [[CrossRef](#)]
10. Okuda-Shimazaki, J.; Yoshida, H.; Sode, K. FAD Dependent Glucose Dehydrogenases—Discovery and Engineering of Representative Glucose Sensing Enzymes-. *Bioelectrochemistry* **2020**, *132*, 107414. [[CrossRef](#)]
11. Igarashi, S.; Ohtera, T.; Yoshida, H.; Witarto, A.B.; Sode, K. Construction and Characterization of Mutant Water-Soluble PQQ Glucose Dehydrogenases with Altered Km Values—Site-Directed Mutagenesis Studies on the Putative Active Site. *Biochem. Biophys. Res. Commun.* **1999**, *264*, 820–824. [[CrossRef](#)] [[PubMed](#)]
12. Haque, A.J.; Nandhakumar, P.; Yang, H. Specific and Rapid Glucose Detection Using NAD-dependent Glucose Dehydrogenase, Diaphorase, and Osmium Complex. *Electroanalysis* **2019**, *31*, 876–882. [[CrossRef](#)]
13. Yamaoka, H.; Yamashita, Y.; Ferri, S.; Sode, K. Site Directed Mutagenesis Studies of FAD-Dependent Glucose Dehydrogenase Catalytic Subunit of Burkholderia Cepacia. *Biotechnol. Lett.* **2008**, *30*, 1967–1972. [[CrossRef](#)] [[PubMed](#)]
14. Milton, R.D.; Giroud, F.; Thumser, A.E.; Minter, S.D.; Slade, R.C.T. Glucose Oxidase Progressively Lowers Bilirubin Oxidase Bioelectrocatalytic Cathode Performance in Single-Compartment Glucose/Oxygen Biological Fuel Cells. *Electrochim. Acta* **2014**, *140*, 59–64. [[CrossRef](#)]
15. Özgeriş, F.B.; Yeltekin, A.Ç.; Ucar, A.; Çağlar, Ö.; Parlak, V.; Arslan, M.E.; Türkez, H.; Atamanalp, M.; Alak, G. Toxic Releases and Exposure Assessment: A Multi-Endpoint Approach in Fish for Ferrocene Toxicity. *Process Saf. Environ. Prot.* **2023**, *169*, 636–645. [[CrossRef](#)]
16. Loew, N.; Tsugawa, W.; Nagae, D.; Kojima, K.; Sode, K. Mediator Preference of Two Different FAD-Dependent Glucose Dehydrogenases Employed in Disposable Enzyme Glucose Sensors. *Sensors* **2017**, *17*, 2636. [[CrossRef](#)]
17. Okurita, M.; Suzuki, N.; Loew, N.; Yoshida, H.; Tsugawa, W.; Mori, K.; Kojima, K.; Klonoff, D.C.; Sode, K. Engineered Fungus Derived FAD-Dependent Glucose Dehydrogenase with Acquired Ability to Utilize Hexaammineruthenium(III) as an Electron Acceptor. *Bioelectrochemistry* **2018**, *123*, 62–69. [[CrossRef](#)]
18. Ishida, K.; Orihara, K.; Muguruma, H.; Iwasa, H.; Hiratsuka, A.; Tsuji, K.; Kishimoto, T. Comparison of Direct and Mediated Electron Transfer in Electrodes with Novel Fungal Flavin Adenine Dinucleotide Glucose Dehydrogenase. *Anal. Sci. Int. J. Jpn. Soc. Anal. Chem.* **2018**, *34*, 783–787. [[CrossRef](#)]
19. Nakabayashi, Y.; Omayu, A.; Yagi, S.; Nakamura, K.; Motonaka, J. Evaluation of Osmium(II) Complexes as Electron Transfer Mediators Accessible for Amperometric Glucose Sensors. *Anal. Sci.* **2001**, *17*, 945–950. [[CrossRef](#)]
20. Zakeeruddin, S.M.; Fraser, D.M.; Nazeeruddin, M.-K.; Grätzel, M. Towards Mediator Design: Characterization of Tris-(4,4'-Substituted-2,2'-Bipyridine) Complexes of Iron(II), Ruthenium(II) and Osmium(II) as Mediators for Glucose Oxidase of *Aspergillus Niger* and Other Redox Proteins. *J. Electroanal. Chem.* **1992**, *337*, 253–283. [[CrossRef](#)]
21. Nazeeruddin, M.K.; Zakeeruddin, S.M.; Kalyanasundaram, K. Enhanced Intensities of the Ligand-to-Metal Charge-Transfer Transitions in Ruthenium(III) and Osmium(III) Complexes of Substituted Bipyridines. *J. Phys. Chem.* **1993**, *97*, 9607–9612. [[CrossRef](#)]
22. Kim, H.-H.; Mano, N.; Zhang, Y.; Heller, A. A Miniature Membrane-Less Biofuel Cell Operating under Physiological Conditions at 0.5 V. *J. Electrochem. Soc.* **2003**, *150*, A209. [[CrossRef](#)]
23. Jeon, W.-Y.; Lee, C.-J.; Kim, H.-H.; Choi, Y.-B.; Lee, B.-H.; Jo, H.-J.; Jeon, S.-Y. Glucose Detection via Ru-Mediated Catalytic Reaction of Glucose Dehydrogenase. *Adv. Mater. Lett.* **2018**, *9*, 220–224. [[CrossRef](#)]



24. Beck, R.W.; Bergenstal, R.M.; Riddlesworth, T.D.; Kollman, C.; Li, Z.; Brown, A.S.; Close, K.L. Validation of Time in Range as an Outcome Measure for Diabetes Clinical Trials. *Diabetes Care* **2019**, *42*, 400–405. [[CrossRef](#)]
25. American Diabetes Association Professional Practice Committee. 7. Diabetes Technology: Standards of Medical Care in Diabetes—2022. *Diabetes Care* **2022**, *45*, S97–S112. [[CrossRef](#)]
26. Lucarelli, F.; Ricci, F.; Caprio, F.; Valgimigli, F.; Scuffi, C.; Moscone, D.; Palleschi, G. GlucoMen Day Continuous Glucose Monitoring System: A Screening for Enzymatic and Electrochemical Interferents. *J. Diabetes Sci. Technol.* **2012**, *6*, 1172–1181. [[CrossRef](#)]
27. Wisniewski, N.; Moussy, F.; Reichert, W.M. Characterization of Implantable Biosensor Membrane Biofouling. *Fresenius' J. Anal. Chem.* **2000**, *366*, 611–621. [[CrossRef](#)]
28. Moon, B.-U.; Koster, S.; Wientjes, K.J.C.; Kwapiszewski, R.M.; Schoonen, A.J.M.; Westerink, B.H.C.; Verpoorte, E. An Enzymatic Microreactor Based on Chaotic Micromixing for Enhanced Amperometric Detection in a Continuous Glucose Monitoring Application. *Anal. Chem.* **2010**, *82*, 6756–6763. [[CrossRef](#)]
29. Klonoff, D.C. Continuous Glucose Monitoring. *Diabetes Care* **2005**, *28*, 1231–1239. [[CrossRef](#)]
30. Feldman, B.; Brazg, R.; Schwartz, S.; Weinstein, R. A Continuous Glucose Sensor Based on Wired Enzyme<sup>TM</sup> Technology—Results from a 3-Day Trial in Patients with Type 1 Diabetes. *Diabetes Technol. Ther.* **2003**, *5*, 769–779. [[CrossRef](#)]
31. Tamada, J.A.; Garg, S.; Jovanovic, L.; Pitzer, K.R.; Fermi, S.; Potts, R.O. The Cygnus Research Team Noninvasive Glucose Monitoring: Comprehensive Clinical Results. *JAMA* **1999**, *282*, 1839. [[CrossRef](#)] [[PubMed](#)]
32. Sreenan, S.; Andersen, M.; Thorsted, B.L.; Wolden, M.L.; Evans, M. Increased Risk of Severe Hypoglycemic Events with Increasing Frequency of Non-Severe Hypoglycemic Events in Patients with Type 1 and Type 2 Diabetes. *Diabetes Ther.* **2014**, *5*, 447–458. [[CrossRef](#)] [[PubMed](#)]
33. Tang, L.; Chang, S.J.; Chen, C.-J.; Liu, J.-T. Non-Invasive Blood Glucose Monitoring Technology: A Review. *Sensors* **2020**, *20*, 6925. [[CrossRef](#)] [[PubMed](#)]
34. Acciaroli, G.; Vettoretti, M.; Facchinetti, A.; Sparacino, G. Calibration of Minimally Invasive Continuous Glucose Monitoring Sensors: State-of-The-Art and Current Perspectives. *Biosensors* **2018**, *8*, 24. [[CrossRef](#)]
35. Yamamoto, K.; Zeng, H.; Shen, Y.; Ahmed, M.; Kato, T. Evaluation of an Amperometric Glucose Biosensor Based on a Ruthenium Complex Mediator of Low Redox Potential. *Talanta* **2005**, *66*, 1175–1180. [[CrossRef](#)]
36. Gerard, M. Application of Conducting Polymers to Biosensors. *Biosens. Bioelectron.* **2002**, *17*, 345–359. [[CrossRef](#)]
37. Wilson, N.G.; McCreedy, T.; Greenway, G.M. In-Situ Immobilisation of Glucose Oxidase on a Novel Microporous Silica Support. *Analyst* **2000**, *125*, 237–239. [[CrossRef](#)]
38. Liu, B.; Hu, R.; Deng, J. Fabrication of an Amperometric Biosensor Based on the Immobilization of Glucose Oxidase in a Modified Molecular Sieve Matrix. *Analyst* **1997**, *122*, 821–826. [[CrossRef](#)]
39. DeSantis, G.; Jones, J.B. Chemical Modification of Enzymes for Enhanced Functionality. *Curr. Opin. Biotechnol.* **1999**, *10*, 324–330. [[CrossRef](#)]
40. Polizzi, K.M.; Bommarius, A.S.; Broering, J.M.; Chaparro-Riggers, J.F. Stability of Biocatalysts. *Curr. Opin. Chem. Biol.* **2007**, *11*, 220–225. [[CrossRef](#)]
41. Qiu, J.-D.; Zhou, W.-M.; Guo, J.; Wang, R.; Liang, R.-P. Amperometric Sensor Based on Ferrocene-Modified Multiwalled Carbon Nanotube Nanocomposites as Electron Mediator for the Determination of Glucose. *Anal. Biochem.* **2009**, *385*, 264–269. [[CrossRef](#)] [[PubMed](#)]
42. Togo, M.; Takamura, A.; Asai, T.; Kaji, H.; Nishizawa, M. An Enzyme-Based Microfluidic Biofuel Cell Using Vitamin K3-Mediated Glucose Oxidation. *Electrochim. Acta* **2007**, *52*, 4669–4674. [[CrossRef](#)]
43. An, N.; Zhou, C.H.; Zhuang, X.Y.; Tong, D.S.; Yu, W.H. Immobilization of Enzymes on Clay Minerals for Biocatalysts and Biosensors. *Appl. Clay Sci.* **2015**, *114*, 283–296. [[CrossRef](#)]
44. De Lumley-Woodyear, T.; Rocca, P.; Lindsay, J.; Dror, Y.; Freeman, A.; Heller, A. Polyacrylamide-Based Redox Polymer for Connecting Redox Centers of Enzymes to Electrodes. *Anal. Chem.* **1995**, *67*, 1332–1338. [[CrossRef](#)] [[PubMed](#)]
45. Jeon, W.-Y.; Choi, Y.-B.; Kim, H.-H. Ultrasonic Synthesis and Characterization of Poly(Acrylamide)-Co-Poly(Vinylimidazole)@MWCNTs Composite for Use as an Electrochemical Material. *Ultrason. Sonochem.* **2018**, *43*, 73–79. [[CrossRef](#)]
46. Csoeregi, E.; Schmidtke, D.W.; Heller, A. Design and Optimization of a Selective Subcutaneously Implantable Glucose Electrode Based on “Wired” Glucose Oxidase. *Anal. Chem.* **1995**, *67*, 1240–1244. [[CrossRef](#)]
47. Gregg, B.A.; Heller, A. Cross-Linked Redox Gels Containing Glucose Oxidase for Amperometric Biosensor Applications. *Anal. Chem.* **1990**, *62*, 258–263. [[CrossRef](#)]
48. Mano, N.; Heller, A. Detection of Glucose at 2 fM Concentration. *Anal. Chem.* **2005**, *77*, 729–732. [[CrossRef](#)]
49. Olejnik, A.; Karczewski, J.; Dołęga, A.; Siuzdak, K.; Grochowska, K. Novel Approach to Interference Analysis of Glucose Sensing Materials Coated with Nafion. *Bioelectrochemistry* **2020**, *135*, 107575. [[CrossRef](#)]
50. Pruna, R.; Palacio, F.; Martínez, M.; Blázquez, O.; Hernández, S.; Garrido, B.; López, M. Organosilane-Functionalization of Nanostructured Indium Tin Oxide Films. *Interface Focus* **2016**, *6*, 20160056. [[CrossRef](#)]
51. Kamra, T.; Chaudhary, S.; Xu, C.; Johansson, N.; Montelius, L.; Schnadt, J.; Ye, L. Covalent Immobilization of Molecularly Imprinted Polymer Nanoparticles Using an Epoxy Silane. *J. Colloid Interface Sci.* **2015**, *445*, 277–284. [[CrossRef](#)] [[PubMed](#)]
52. Innocenzi, P.; Kidchob, T.; Yoko, T. Hybrid Organic-Inorganic Sol-Gel Materials Based on Epoxy-Amine Systems. *J. Sol-Gel Sci. Technol.* **2005**, *35*, 225–235. [[CrossRef](#)]

53. Balaji, J.; Sethuraman, M.G. Corrosion Protection of Copper with 3-Glycidoxypropyltrimethoxysilane-Based Sol–Gel Coating through 3-Amino-5-Mercapto-1,2,4-Triazole Doping. *Res. Chem. Intermed.* **2016**, *42*, 1315–1328. [CrossRef]
54. Hossain, M.M.; Morshed, J.; Tsujimura, S. Designing a Cross-Linked Redox Network for a Mediated Enzyme-Based Electrode. *Chem. Commun.* **2021**, *57*, 6999–7002. [CrossRef]
55. Zafar, M.N.; Wang, X.; Sygmund, C.; Ludwig, R.; Leech, D.; Gorton, L. Electron-Transfer Studies with a New Flavin Adenine Dinucleotide Dependent Glucose Dehydrogenase and Osmium Polymers of Different Redox Potentials. *Anal. Chem.* **2012**, *84*, 334–341. [CrossRef]
56. Ohara, T.J.; Rajagopalan, R.; Heller, A. “Wired” Enzyme Electrodes for Amperometric Determination of Glucose or Lactate in the Presence of Interfering Substances. *Anal. Chem.* **1994**, *66*, 2451–2457. [CrossRef]
57. Streeter, I.; Wildgoose, G.G.; Shao, L.; Compton, R.G. Cyclic Voltammetry on Electrode Surfaces Covered with Porous Layers: An Analysis of Electron Transfer Kinetics at Single-Walled Carbon Nanotube Modified Electrodes. *Sens. Actuators B Chem.* **2008**, *133*, 462–466. [CrossRef]
58. Solanki, P.R.; Kaushik, A.; Ansari, A.A.; Sumana, G.; Malhotra, B.D. Zinc Oxide-Chitosan Nanobiocomposite for Urea Sensor. *Appl. Phys. Lett.* **2008**, *93*, 163903. [CrossRef]
59. Van Benschoten, J.J.; Lewis, J.Y.; Heineman, W.R.; Roston, D.A.; Kissinger, P.T. Cyclic Voltammetry Experiment. *J. Chem. Educ.* **1983**, *60*, 772. [CrossRef]
60. Pekel, N.; Güven, O. Investigation of Complex Formation between Poly(N-Vinyl Imidazole) and Various Metal Ions Using the Molar Ratio Method. *Colloid Polym. Sci.* **1999**, *277*, 570–573. [CrossRef]
61. Verma, A.; Chaudhary, P.; Tripathi, R.K.; Yadav, B.C. The Functionalization of Polyacrylamide with MoS<sub>2</sub> Nanoflakes for Use in Transient Photodetectors. *Sustain. Energy Fuels* **2021**, *5*, 1394–1405. [CrossRef]
62. Pekel, N.; Güven, O. Spectroscopic and Thermal Studies of Poly[( N -Vinylimidazole)-Co-(Maleic Acid)] Hydrogel and Its Quaternized Form. *Polym. Int.* **2008**, *57*, 637–643. [CrossRef]
63. Paris, J.P.; Brandt, W.W. Charge Transfer Luminescence of a Ruthenium(II) Chelate. *J. Am. Chem. Soc.* **1959**, *81*, 5001–5002. [CrossRef]
64. Baldo, M.A.; Daniele, S.; Mazzocchin, G.A. Cyclic Voltammetry at Mercury Microelectrodes. Effects of Mercury Thickness and Scan Rate. *Electrochim. Acta* **1996**, *41*, 811–818. [CrossRef]
65. Wang, X.; Jiang, A.; Hou, T.; Li, F. A Sensitive and Versatile “Signal-on” Electrochemical Aptasensor Based on a Triple-Helix Molecular Switch. *Analyst* **2014**, *139*, 6272–6278. [CrossRef] [PubMed]
66. Kong, D.; Zhao, J.; Tang, S.; Shen, W.; Lee, H.K. Logarithmic Data Processing Can Be Used Justifiably in the Plotting of a Calibration Curve. *Anal. Chem.* **2021**, *93*, 12156–12161. [CrossRef]
67. Takamatsu, S.; Takano, H.; Binh-Khiem, N.; Takahata, T.; Iwase, E.; Matsumoto, K.; Shimoyama, I. Liquid-Phase Packaging of a Glucose Oxidase Solution with Parylene Direct Encapsulation and an Ultraviolet Curing Adhesive Cover for Glucose Sensors. *Sensors* **2010**, *10*, 5888–5898. [CrossRef]
68. EMA ICH Q2(R2) Validation of Analytical Procedures—Scientific Guideline. Available online: <https://www.ema.europa.eu/en/ich-q2r2-validation-analytical-procedures-scientific-guideline> (accessed on 2 July 2023).
69. Lee, I.; Probst, D.; Klonoff, D.; Sode, K. Continuous Glucose Monitoring Systems—Current Status and Future Perspectives of the Flagship Technologies in Biosensor Research-. *Biosens. Bioelectron.* **2021**, *181*, 113054. [CrossRef]
70. Kim, J.; Imani, S.; De Araujo, W.R.; Warchall, J.; Valdés-Ramírez, G.; Paixão, T.R.L.C.; Mercier, P.P.; Wang, J. Wearable Salivary Uric Acid Mouthguard Biosensor with Integrated Wireless Electronics. *Biosens. Bioelectron.* **2015**, *74*, 1061–1068. [CrossRef]
71. Mäkilä, E.; Kirveskari, P. A Study of Ascorbic Acid in Human Saliva. *Arch. Oral Biol.* **1969**, *14*, 1285–1292. [CrossRef]
72. Piechotta, G.; Albers, J.; Hintsche, R. Novel Micromachined Silicon Sensor for Continuous Glucose Monitoring. *Biosens. Bioelectron.* **2005**, *21*, 802–808. [CrossRef] [PubMed]
73. Chinnadayala, S.R.; Park, K.D.; Cho, S. Editors’ Choice—Review—In Vivo and In Vitro Microneedle Based Enzymatic and Non-Enzymatic Continuous Glucose Monitoring Biosensors. *ECS J. Solid State Sci. Technol.* **2018**, *7*, Q3159–Q3171. [CrossRef]
74. Invernale, M.A.; Tang, B.C.; York, R.L.; Le, L.; Hou, D.Y.; Anderson, D.G. Microneedle Electrodes Toward an Amperometric Glucose-Sensing Smart Patch. *Adv. Healthc. Mater.* **2014**, *3*, 338–342. [CrossRef] [PubMed]
75. Valdés-Ramírez, G.; Li, Y.-C.; Kim, J.; Jia, W.; Bandodkar, A.J.; Nuñez-Flores, R.; Miller, P.R.; Wu, S.-Y.; Narayan, R.; Windmiller, J.R.; et al. Microneedle-Based Self-Powered Glucose Sensor. *Electrochem. Commun.* **2014**, *47*, 58–62. [CrossRef]
76. Hwa, K.-Y.; Subramani, B.; Chang, P.-W.; Chien, M.; Huang, J.-T. Transdermal Microneedle Array-Based Sensor for Real Time Continuous Glucose Monitoring. *Int. J. Electrochem. Sci.* **2015**, *10*, 2455–2466. [CrossRef]
77. Windmiller, J.R.; Valdés-Ramírez, G.; Zhou, N.; Zhou, M.; Miller, P.R.; Jin, C.; Brozik, S.M.; Polsky, R.; Katz, E.; Narayan, R.; et al. Bicomponent Microneedle Array Biosensor for Minimally-Invasive Glutamate Monitoring. *Electroanalysis* **2011**, *23*, 2302–2309. [CrossRef]

**Disclaimer/Publisher’s Note:** The statements, opinions and data contained in all publications are solely those of the individual author(s) and contributor(s) and not of MDPI and/or the editor(s). MDPI and/or the editor(s) disclaim responsibility for any injury to people or property resulting from any ideas, methods, instructions or products referred to in the content.